Research Article | Vol. 27, No. 14 | 8 Jul 2019 | OPTICS EXPRESS 19996
Optics EXPRESS

Digital monitoring and compensation of MDL based on higher-order Poincaré spheres

G. M. FERNANDES,[1,*] N. J. MUGA,[1] AND A. N. PINTO[1,2]

[1] *Instituto de Telecomunicações, Campus Universitário de Santiago, 3810-193 Aveiro, Portugal*
[2] *Department of Electronics, Telecommunications and Informatics, University of Aveiro, Portugal*
[*] *gfernandes@av.it.pt*

Abstract: We present a digital technique able to monitor and compensate for the mode-dependent losses (MDL) in space-division multiplexing (SDM) transmission systems. The working principle of the technique is based on the analysis of the received signal samples in the higher-order Poincaré spheres (HoPs). When an arbitrary pair of tributaries is represented in the respective HoPs, the effect of the MDL can be modeled as a simple shift of the constellation points in a such sphere. Therefore, the MDL can be estimated by computing those shifts over all the HoPs and the induced signal distortions can be compensated by re-centering all the constellations in the respective HoPs. It should be highlighted that the proposed technique is scalable with an arbitrary number of spatial channels, modulation format agonistic and free of training sequences. The HoPs-based MDL monitoring (compensation) technique allows the MDL estimation (compensation) up to values of ≈ 6 dB. The proposed technique can partially compensate the MDL distortion, making a MDL sensitive algorithm in an insensitive one. When the proposed technique assists a HoPs-based space-demultiplexing algorithm, it provides signal-to-noise ratio (SNR) enhancements of 2, 4 and 8 dB for PM-QPSK, PM-16QAM and PM-64QAM signals, respectively, for the particular case of a SDM-based transmission system with a spatial diversity of 2 and 2 dB of MDL.

1. Introduction

The space-division multiplexing (SDM) has been proposed to increase the aggregate bit-rate transmitted through a single optical fiber using independent cores of a multicore fiber or orthogonal modes of a few-mode fiber (FMF) or a coupled-core multicore fiber (CC-MCF) [1]. However, these systems suffer from mode dependent gains or losses, collectively referred to as mode-dependent losses (MDL), which acts as a fundamental limiting factor to the maximum achievable aggregate bit-rate of SDM transmission systems [1–4]. In transmission systems based on standard single-mode fiber (SSMF), the polarization-dependent losses (PDL), the analogous effect to MDL in the single-mode case, is monitored and compensated at the coherent optical receiver by means of advanced digital signal processing (DSP) [5, 6]. For instance, in SSMF-based transmission systems, several PDL compensation techniques have been proposed in order to improve the performance of other PDL sensitive DSP subsystems [7]. In optical coherent receivers with MDL-sensitive DSP, the development of algorithms and techniques with faster adaptation and tolerable computational complexity capable of compensating for MDL will certainly play a fundamental role. On the other hand, the overall performance of the SDM transmission systems will also benefit from MDL monitoring techniques.

In transmission systems over SSMF, the coherent receivers employ multiple-input multiple-output (MIMO) equalization to compensate for stochastic impairments [5], including polarization rotations through polarization-demultiplexing (PolDemux) algorithms. Although several PolDemux algorithms have been reported [5], Stokes-based PolDemux has attracted the attention of the scientific community as it presents important advantages, e.g., transparency to the modulation format and robustness to phase fluctuations and frequency offsets [8, 9]. Several approaches of Stokes-based PolDemux algorithms have been experimentally demonstrated [10, 11], including

#362502 https://doi.org/10.1364/OE.27.019996
Journal © 2019 Received 20 Mar 2019; revised 7 Jun 2019; accepted 8 Jun 2019; published 5 Jul 2019

Optics EXPRESS

a real-time implementation on field-programmable gate array (FPGA) of a dual-polarization coherent ultra-dense wavelength division multiplexing (UDWDM) system [12]. In Stokes-based PolDemux algorithms, the spatial orientation of the best fit plane, defined by the received samples in the Stokes space, can be employed to compute the demultiplexing matrix [7, 10, 13]. If the transmission channel is free of PDL, then the best fit plane contains the center of the Poincaré sphere. In the presence of PDL, however, the constellation is shifted from the center of the Poincaré sphere [14]. Hence, the PDL can be monitored by assessing the aforementioned shift and the induced signal distortions can be also compensated by re-centering the constellation at the origin of the Poincaré sphere. This procedure permits to compute an enhanced inverse channel matrix, improving the signal-to-noise ratio (SNR) of the post-processed signal [7, 14].

Higher-order Poincaré spheres (HoPs) are commonly defined as a full set of geometric representations of a given vector space, where a pair of orthogonal states is represented in a single sphere, likewise the Bloch and the Poincaré spheres [15–18]. DSP subsystems based on the signal representation in HoPs, were also recently proposed for SDM transmission systems [19, 20, 22]. Employing such signal representation, the task of space-demultiplexing (SpDemux) is accomplished without requiring training sequences, and with transparency to modulation formats and higher robustness against phase fluctuations and frequency offsets [19,20]. The demultiplexing matrix for an arbitrary pair of tributaries is calculated using the spatial orientation of best fit plane, while the demultiplexing matrix for the entire signal is computed by progressively demultiplexing all the pairs of tributaries [19]. However, this matrix depends on the sequence of HoPs or pair of tributaries considered. In [19], the optimized sequence of HoPs is found by analyzing all possible sequences and choosing the one with the best fittings. In [20], an iterative method to found a suitable sequence of HoPs was proposed; tremendously reducing the computational complexity and improving the convergence speed. However, the performance of such SpDemux algorithms will certainly benefit from the availability of new impairment compensation techniques. In particular, techniques whose principle of operation are also based on the signal representation in HoPs.

In this paper, we propose a digital HoPs-based MDL monitoring technique which is scalable for a large number of spatial channels, modulation format agnostic and free of training sequences. Furthermore, we also propose a HoPs-based MDL compensation technique that improves the performance of DSP subsystems sensitive to MDL. In particular, we show that the previously proposed HoPs-based SpDemux algorithm [20] is sensitive to MDL, which results in a non-negligible SNR penalty of the post-processed signal. However, when such SpDemux algorithm is assisted by the MDL compensation technique proposed in this work, it provides a SNR gain of ≈ 2, 4 and 8 dB for a polarization-multiplexed (PM)-quadrature phase-shift keying (QPSK), 16 quadrature amplitude modulation (QAM) and 64QAM signals, respectively.

The remainder of this paper is organized as follows. In section 2, we briefly introduce the signal representation in HoPs. The proposed MDL monitoring and compensation technique is carefully described in section 3. In section 4, the proposed technique is analyzed in terms of relative error on the MDL vector estimation, convergence speed and SNR enhancements of the post-processed signal. Finally, the main conclusions are presented in section 5.

2. Higher-order Poincaré spheres

In the following sections, we use the Dirac notation to represent the signal in the Jones space,

$$|\psi\rangle = (\upsilon_1, \upsilon_2, ...\upsilon_h, ...\upsilon_{2n})^T \,, \tag{1}$$

with

$$\upsilon_j(z,t) = a_j(z,t)e^{-i(\omega t+\varphi_j)}, \tag{2}$$

being υ_j the electric field for the jth tributary signal, with $j = 1, ..., 2n$, where n denotes the number of spatial channels. The subscript index T denotes transpose, the parameters t and

Optics EXPRESS

z represents the temporal and the longitudinal coordinates, respectively, and ω is the angular frequency. For a given tributary signal, the envelop amplitude is given by a_j and the phase is represented by φ_j. It should be noted that in Eq. (1) each spatial channel supports a PM signal.

The entire signal can be represented in $g_s = \binom{2n}{2}$ HoPs with the Stokes vector written as [19]

$$\Psi_l^{(f,g)} = \langle\psi|\, \mathbf{\Lambda}_l^{(f,g)}\, |\psi\rangle\ , \tag{3}$$

being $\langle\cdot|$ the complex conjugated of $|\cdot\rangle$, with the indexes $l = 1, 2, 3$, $f = 1, 2..., 2n-1$ and $g = f+1, ..., 2n$. In Eq. (3), the superscript g and f denotes the υ_f and υ_g tributaries, respectively, selected from Eq. (1). The signal representation based on HoPs followed in [19] comprises two distinct kind of spheres, accounting in that way for the cases of intramode and intermode tributary pairing. For each HoPs, the "Pauli spin vector" is given by [19]

$$\vec{\mathbf{\Lambda}}^{(f,g)} = [\mathbf{\Lambda}_1^{(f,g)}, \mathbf{\Lambda}_2^{(f,g)}, \mathbf{\Lambda}_3^{(f,g)}]^T\ . \tag{4}$$

In the following description of the "Pauli spin vector", the values g and f are related with the tributary signal, according to Eq. (1), and with the writing of the $\mathbf{\Lambda}$ matrices itself. The coefficient $\mathbf{\Lambda}(g, f)$ denotes the value of the matrix $\mathbf{\Lambda}$ for the g line and a f column. The matrix, $\mathbf{\Lambda}_1^{(f,g)}$, is written by considering the elements $\mathbf{\Lambda}_1^{(f,g)}(f, f)$ and $\mathbf{\Lambda}_1^{(f,g)}(g, g)$ in the main diagonal equal to $\sqrt{n}$ (or $\kappa\sqrt{n}$) in the intramode (or intermode) case. The remaining elements of the matrix are set to zero. It should be noticed that in this paper, and as explained in the following paragraph, the parameter κ is not considered in the write of the Pauli spin vector. The matrix $\mathbf{\Lambda}_2^{(f,g)}$ is written by considering the elements outside of the main diagonal, $\mathbf{\Lambda}_2^{(f,g)}(f, g)$ and $\mathbf{\Lambda}_2^{(f,g)}(g, f)$, equal to $\sqrt{n}$ and equal to $-\sqrt{n}$, respectively, and the remaining elements are set to zero. Lastly, the matrix, $\mathbf{\Lambda}_3^{(f,g)}$, is written by considering the elements $\mathbf{\Lambda}_3^{(f,g)}(f, g)$ equal to $i\sqrt{n}$, with $i = \sqrt{-1}$, and the symmetric element equal to $-i\sqrt{n}$; the remaining elements are set to zero. Although the construction of $\vec{\mathbf{\Lambda}}^{(f,g)}$ may result non-obvious, its understanding for scenarios of few modes is becomes straightforward. A detailed description of $\vec{\mathbf{\Lambda}}^{(f,g)}$ for the particular case of two spatial channels is given elsewhere [19].

The Stokes parameters for the generalized Stokes space can be directly written as a linear combination of the Stokes parameters for the g_s HoPs, if the Pauli spin vector is written as above [19, 21]. Such property can be very useful to estimate the maximum available aggregated bit-rate transmitted through the channel [2]. However, for the purpose of DSP, or more precisely MDL monitoring and compensation, the Pauli spin vector can be computed neglecting the parameter κ, thus simplifying the computation of the Pauli spin vector and further calculations. This simplification will be clearly explained along the subsection 3.1.

3. MDL monitoring and compensation technique

Throughout this section, we introduce the operation principle behind the HoPs-based MDL monitoring and compensation technique. Firstly, we assume a particular transmission link where MDL is the unique channel impairment. When two given tributaries are represented in the respective HoPs, we show that the gain/losses power imbalance induce a shift of the central point of the constellation through the Ψ_1 axis. Therefore, such power imbalance can be compensated by re-centering the constellation. The MDL-induced signal distortions can be fully compensated by repeating the above procedure for all HoPs. Secondly, the proposed technique is extended to the general case, in which crosstalk and MDL coexist. In that case, the central point of the constellation can take an arbitrary position on the HoPs and thus a set of rotations and translations must be considered to re-center the constellation.

Optics EXPRESS

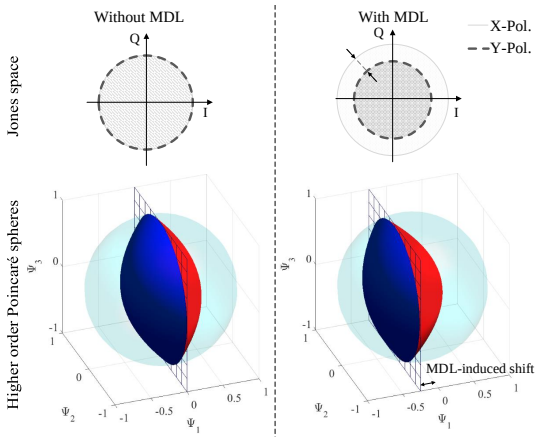

Fig. 1. Upper row: schematic representation of two tributaries containing arbitrary modulation format in the Jones space without and with MDL, left and right, respectively. Lower row: schematic representation of two tributaries containing arbitrary modulation formats in the HoPs with and without MDL, left and right, respectively.

3.1. MDL monitoring and compensation: channel only with MDL

We start with the simplest case: the SDM link is only affect by MDL, i.e., crosstalk and dispersion are not taken into account. Assuming a transmission system with a spatial diversity of 2, the channel transfer matrix can be written as

$$\mathbf{H} = \mathrm{diag}\{\rho_1, \rho_2, \rho_3, \rho_4\}, \tag{5}$$

where ρ_j^2, with $j = 1, \ldots 4$, is the gain/loss for the jth tributary, and diag$\{\cdot\}$ denotes a diagonal matrix. For the sake of convenience, in the following sections, the peak-to-peak MDL is chosen as the metric to carry out the performance analyses of the proposed algorithm. For this particular case, the peak-to-peak MDL is given by [1,4],

$$\mathrm{MDL_{P\text{-}P}} = 10 \log \left(\max\{\vec{\Gamma}\}/\min\{\vec{\Gamma}\}\right). \tag{6}$$

with the max$\{\cdot\}$ and min$\{\cdot\}$ being the elements with the maximum and the minimum value of $\vec{\Gamma} = (\rho_1, \rho_2, \rho_3, \rho_4)^2$, respectively (i.e., the eigenvalues of the channels transfer matrix). However, the MDL on SDM transmission systems can also be described using other metrics, such as the MDL vector defined by means of the generalized Pauli spin vector [2] and the root-mean-square (rms) of the gain/loss power imbalances [4].

Without loss of generality, the operation principle of our technique is demonstrated for the first and second tributaries represented in the respective HoPs. However, the same results can be achieved for the remaining pairs of tributaries following a similar approach. For this purpose, we may assume that only a single tributary signal (the second one) is modulated, while the remaining tributaries have constant phase and amplitude. The hypothetical complex-modulation format of the second tributary is assumed to be confined to an unit circle in the Jones space. Notice that such assumptions do not impose any limitation to the transmission system [8]. In the Jones space, the described signal can be written as

$$|\psi\rangle = \left(1, re^{\theta}, 1, 1\right)^T, \tag{7}$$

with $0 < \theta \leq 2\pi$ and $0 < r \leq 1$. By using Eq. (7) into Eq. (3), the following set of parametric

Optics EXPRESS

equations are obtained

$$\Psi_1^{(1,2)} = \langle\psi|\,\mathbf{\Lambda}_1^{(1,2)}\,|\psi\rangle = \sqrt{n}[(1-r^2) - \rho^{(1,2)}(1+r^2)], \tag{8a}$$

$$\Psi_2^{(1,2)} = \langle\psi|\,\mathbf{\Lambda}_2^{(1,2)}\,|\psi\rangle = 2r\sqrt{n}\sqrt{1+\rho^{(1,2)}}\sqrt{1-\rho^{(1,2)}}\cos(\delta_{1,2}), \tag{8b}$$

$$\Psi_3^{(1,2)} = \langle\psi|\,\mathbf{\Lambda}_3^{(1,2)}\,|\psi\rangle = 2r\sqrt{n}\sqrt{1+\rho^{(1,2)}}\sqrt{1-\rho^{(1,2)}}\sin(\delta_{1,2}). \tag{8c}$$

When represented in the respective HoPs, Eq. (8) form a paraboloidal surface (see Fig. 1(a), red surface). If the tributaries 1 and 2 in Eq. (7) are exchanged, i.e., the first tributary carries the above mentioned hypothetical modulation format and the other tributaries assume a constant value, then the respective paraboloidal surface is flipped (see Fig. 1(a), blue surface). Afterwards, the signal is made pass through an element with MDL and the lens-like object is shifted along the axis $\Psi_1^{(1,2)}$ by a maximum value of $2\sqrt{n}\rho^{(1,2)}$. Thus, the parameter $\rho^{(1,2)}$ can be estimated from the plane containing the boundary between both paraboloidal surfaces,

$$\rho^{(1,2)} = -\frac{d^{(1,2)}}{2\sqrt{n}}, \tag{9}$$

where $d^{(1,2)}$ is given by the average value of $\langle\Psi_1^{(1,2)}\rangle$ for a given set of samples. If parameter κ was considered in the writing of the Pauli spin vector, the parameter $\Psi_1^{(1,2)}$ and the left side of Eq. (8) would be also affected by the aforementioned parameters; canceling each other. In Eq. (8) the Stokes parameter, $\Psi_1^{(1,2)}$ are independent of the phase difference, $\delta_{1,2}$, the carrier frequency and its fluctuations [8]. Therefore, such kind of algorithms tends to be robust against frequency offsets and phase fluctuations; analogously to the Stokes-space based PolDemux algorithms in the single mode case [11]. Since the signal requires g_s HoPs to be fully described in such representation, an accurate assessment of the MDL vector requires the analysis of gain/losses power imbalance over all the HoPs. In that way, the inverse channel matrix Eq. (5) is rewritten as

$$\mathbf{H} = \prod_{f=1}^{n-1}\prod_{g=f+1}^{n}\mathbf{T}^{(f,g)}, \tag{10}$$

with the matrix $\mathbf{T}^{(f,g)}$ accounting for the power imbalance between the f and g tributaries. The matrix $\mathbf{T}^{(f,g)}$ can be fully calculated by analyzing the received signal in the respective HoPs. As in the single-mode case, the g_s matrices $\mathbf{T}^{(f,g)}$, henceforward called of translation matrices, can be written as the following diagonal matrix,

$$\mathbf{T}^{(f,g)}(k,l) = \begin{cases} \sqrt{1-\rho^{(f,g)}} & \text{if } k=g, l=g \\ \sqrt{1+\rho^{(f,g)}} & \text{if } k=f, l=f \\ 1 & \text{if } k=l \text{ and } k,l\neq g,f \\ 0 & \text{otherwise}, \end{cases} \tag{11}$$

with the parameter $\rho^{(f,g)}$ accounting for the gain/loss power imbalance between the g and f tributaries. We assume that $\rho^{(f,g)}$ can be independently calculated for all HoPs from the received samples. With this in mind, we redefine the optical power imbalance between a given pair of tributaries as

$$\rho^{(f,g)} = -\frac{\max\{\rho_f,\rho_g\}^2 - \min\{\rho_f,\rho_g\}^2}{2n_k\sqrt{n}}, \tag{12}$$

with n_k denoting a normalization parameter. As all the parameters $\rho^{(f,g)}$ are directly estimated from the received signal, the calculated inverse channel matrix receives several repeated

Optics EXPRESS

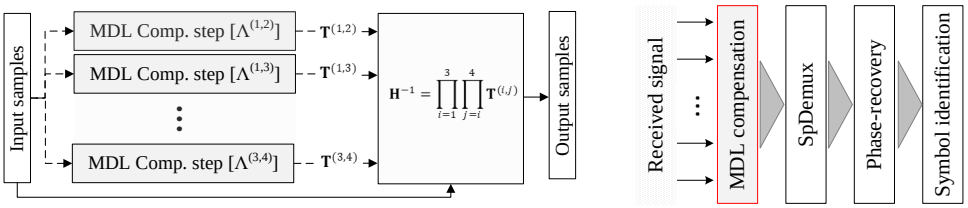

Fig. 2. (a) Schematic of MDL monitoring and compensation technique. (b) Schematic of DSP subsystems considered at the optical coherent receiver.

contributions for the same MDL coefficient; hence over-estimating the eigenvalues of the channel transfer matrix. In that way, we introduce the parameter n_k to compensate for such repeated contributions. Note that, n_k only depends on the number of spatial channels considered in the SDM transmission system. For the scenarios analyzed in this paper, the value of n_k scales with n according to $n_k = \sqrt{n}$. However, for the general case, Eq. (10) must be solved in order to calculate n_k. It should be also emphasised that the translations matrices commute and, therefore, the sequence of these matrices can be neglected in the calculation of $\mathbf{H}$. The schematic of the HoPs-based MDL monitoring and compensation technique is shown in Fig. 2(a), in which the "MDL compensation step" denotes the set of operations required to calculate the translation matrix.

3.2. MDL monitoring and compensation: channel with crosstalk and MDL

The signal propagation through a real link is affected by a large number of impairments, e.g., crosstalk and MDL, among others. The conjugation of crosstalk and MDL increases the complexity of the channel model, requesting a more robust and generalized version of the MDL monitoring and compensation technique previously discussed. However, in this subsection, we are going to show that the methodology presented in the previous subsection can be properly enhanced in order to estimate the eigenvalues of the transfer channel matrix in the presence of crosstalk.

Considering a scenario where both crosstalk and MDL are present, the lens-like object representing the signal samples in the HoPs appears rotated (due to crosstalk) and shifted from the origin of the HoPs space (due to MDL). Therefore, the best-fit plane is no longer parallel to the plane defined by $\Psi_1^{(f,g)} = 0$, and the central point of the constellation does not belong to the $\Psi_1^{(f,g)}$ axis. Here, the real value of gains/losses power imbalance is related with the geometric distribution of the signal samples in the HoPs, as follows

$$\rho^{(f,g)} = -\frac{D^{(f,g)}}{2n_k\sqrt{n}a^2}, \tag{13}$$

where a is the average value of the envelope amplitude for both tributaries, and $D^{(f,g)}$ represents the Euclidean distance between the central point of the moved lens-like object, $P^{(f,g)}$, and the origin of the HoPs space, O. Such distance can be easily computed from the coordinates of the central point of the constellation, $P^{(f,g)} = \left(d_1^{(f,g)}, d_2^{(f,g)}, d_3^{(f,g)}\right)$, using:

$$D^{(f,g)} = \overline{P^{(f,g)}O} = \sqrt{\left(d_1^{(f,g)}\right)^2 + \left(d_2^{(f,g)}\right)^2 + \left(d_3^{(f,g)}\right)^2}, \tag{14}$$

where $d_j^{(f,g)} = \langle \Psi_j^{(f,g)}(l) \rangle = \frac{1}{N}\sum_{l=1}^{N} \Psi_j^{(f,g)}(l)$, with $j = 1, 2$ and 3, and N representing the

Optics EXPRESS

number of signal samples used in the computation. Notice that, a significant number of samples N must be considered in order to assure that the center of the constellation, $P^{(f,g)}$, is accurately estimated.

In order to compensate the MDL in the presence of crosstalk, the center of the constellation must be shifted to the origin of the HoPs. For such purpose, a set of rotations and translations matrices are applied to the received samples [7],

$$|\psi\rangle_{out} = \left[\mathbf{U}_2^{(f,g)}(-\theta)\mathbf{T}^{(f,g)}(d_3)\mathbf{U}_2^{(f,g)}(\theta)\right]\left[\mathbf{U}_3^{(f,g)}(-\theta)\mathbf{T}^{(f,g)}(d_2)\mathbf{U}_3^{(f,g)}(\theta)\right]\mathbf{T}^{(f,g)}(d_1)\,|\psi\rangle_{in}\,, \tag{15}$$

with $|\psi\rangle_{in}$ and $|\psi\rangle_{out}$ denoting the signal before and after MDL compensation, respectively. In the Jones space, the rotation matrices $\mathbf{U}_3(\theta)$ and $\mathbf{U}_2(\theta)$ can be written as,

$$\mathbf{U}_3(\theta)^{(g,f)}(k,l) = \begin{cases} \cos(\theta/2) \\ -\sin(\theta/2) \\ \sin(\theta/2) \\ \cos(\theta/2) \\ 1 \\ 0 \end{cases} \quad \text{and} \quad \mathbf{U}_2(\theta)^{(g,f)}(k,l) = \begin{cases} \cos(\theta/2) & \text{if } k=g, l=g \\ i\sin(\theta/2) & \text{if } k=g, l=f \\ i\sin(\theta/2) & \text{if } k=f, l=g \\ \cos(\theta/2) & \text{if } k=f, l=f \\ 1 & \text{if } k=l \text{ and } k,l \neq g,f \\ 0 & \text{otherwise}, \end{cases} \tag{16}$$

respectively. The set of operations performed in Eq. (15) can be summarized as follows: the constellation is shifted by d_1 along the axis $\Psi_1^{(f,g)}$ using $\mathbf{T}^{(f,g)}(d_1)$. Then, the lens-like object is shifted along the axis $\Psi_2^{(f,g)}$. Before this shift, the samples must be rotated of an angle $\theta = \pi/2$ around the axis $\Psi_3^{(f,g)}$ employing $\mathbf{U}_3^{(f,g)}$ and afterwards displaced of d_2 along the axis $\Psi_2^{(f,g)}$. In order to get back the original spatial orientation of the constellation, samples are again rotated by $-\theta$, with $\theta = \pi/2$, applying $\mathbf{U}_3^{(f,g)}$. Lastly, a similar procedure is employed at the third stage, which comprises the shift of samples along the axis $\Psi_3^{(f,g)}$. In this case, the required rotations are made around the axis $\Psi_2^{(f,g)}$.

4. Performance assessment

Usually, CC-MCF and FMF tend to have a large effective area than SSMF. In that way, fiber nonlinearities are neglected, with the channel model being assumed as a linear matrix. Without loss of generality, we are going to consider a SDM-based transmission system with negligible modal dispersion. In practical terms, scenarios of negligible modal dispersion occur in systems with weakly-coupled FMF, in which the distinct orders of the LP modes remain uncoupled while the tributaries signals of a given LP family are coupled [23] or in moderated lengths of CC-MCF with low modal dispersion [24]. Moreover, in SDM transmission systems with non-negligible modal dispersion, additional DSP subsystems placed at the optical coherent receiver can in principle enable the modal dispersion compensation before the space-demultiplexing, as explained in subsection 4.4.

Currently, SDM transmission systems are been proposed for short reach applications [25], where non-negligible MDL can be induced by several elements, including space-(de)multiplexers, reconfigurable optical add-drop multiplexers (ROADM) and the fibers itself. However, the number of in-line amplifiers can be very reduced or even absent. Throughout this paper, we are going to assume that the white noise is injected at the transmitter side, with the exception of subsection 4.3.1, where the impact of the amplified spontaneous emission (ASE) is analyzed.

In the optical coherent receiver, the signal distortions induced by distinct transmission impairments are equalized at different DSP subsystems; for instance, chromatic dispersion and phase noise are compensated by independent DSP subsystems. Usually, the signal distortions

Optics EXPRESS

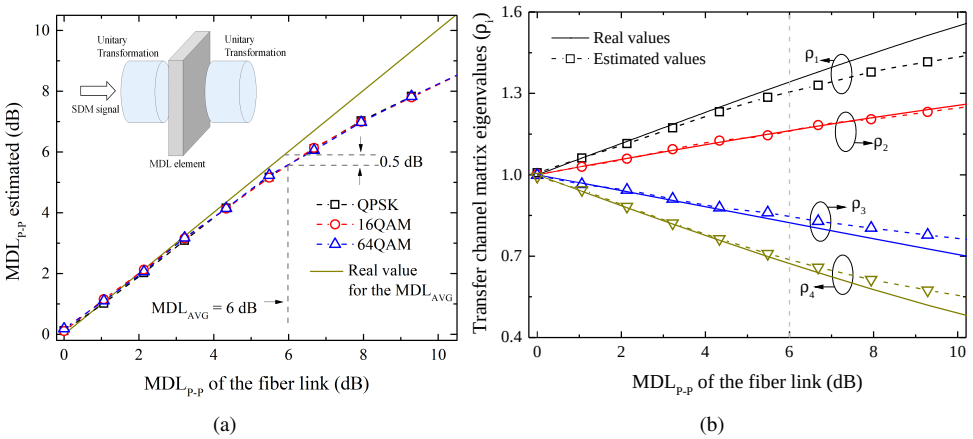

Fig. 3. (a) Estimated value of MDL as a function of the real value of MDL for a transmission system with two spatial channels, considering PM-QPSK, PM-16QAM, and PM-64QAM signal. (b) Components of the MDL vector as a function of the real ones. The four values of ρ are estimated from a PM-QPSK signal.

induced by MDL are compensated by an adaptive equalizer, simultaneously compensating for crosstalk, among other phenomena. In that way, it is assumed that MDL and crosstalk must be jointly compensated, whereas the remaining signal distortions can be previously compensated by other DSP subsystems.

Due to the crosstalk along the propagation, all the tributaries appear mixed at the receiver side. Therefore, and to assure an accurate assessment of the proposed technique, the HoPs-based SpDemux algorithm reported in [20] is used to compensate the crosstalk after the MDL compensation. The performance of the SpDemux is affected by the MDL and, therefore, the MDL compensation must be performed before the SpDemux. It should be emphasized that the MDL monitoring and compensation does not require a previous SpDemux of the received signal because it only comprises the calculation, and subsequent shift, of the center of the constellations in the respective HoPs. After MDL compensation plus SpDemux, a modified Viterbi-Viterbi algorithm is employed to calculate the angle offset resulting from the calculation of the demultiplexing matrix in HoPs. Notice that a large number of samples was employed in the calculations of the aforementioned offset. Lastly, the phase offset is compensated and the SNR is calculated through the average value of the error vector magnitude (EVM) of the post-processed signal. The complete set of DSP subsystems, including MDL compensation and SpDemux, employed at the receiver side for signal recovering are schematically represented in Fig. 2(b).

In the following subsections, we assume a transmission system with two spatial channels (i.e., a 2-core CC-MCF), each spatial channel carrying a pseudorandom bit sequence (PRBS) of 2^{18} bits coded in different complex-modulation formats, including PM-QPSK, PM-16QAM, and PM-64QAM with SNRs of 17, 23 and 30 dB, respectively. The results presented in the following subsections are obtained by averaging over 100 trials, with the exception of Fig. 8.

4.1. Propagation channel

In order to model the signal propagation through a link with SDM, we consider the multi-section propagation model [27]. This model assumes that the link is composed of n_s spans of fiber, which, in turn, are sub-divided in n_{step} sections. The impulse response of the channel, $\mathbf{M}$, is

Optics EXPRESS

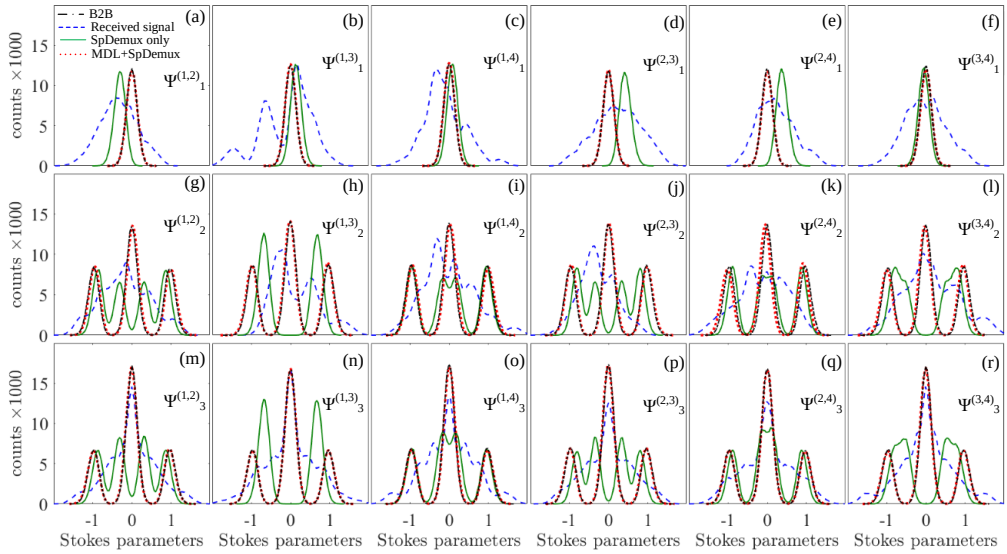

Fig. 4. Stokes parameters histograms for a PM-QPSK signal transmitted through a SDM link with 3 dB of MDL. In black the B2B signal. In blue/green the received signal before/after the SpDemux stage without MDL compensation stage. In red the post-processed signal after MDL compensation plus SpDemux. Lines are used (instead of 500 bars) to smooth the representation of all data in the same plot. (a)-(f): parameter $\Psi_1^{(f,g)}$, (g)-(l): parameter $\Psi_2^{(f,g)}$ and (m)-(r): parameter $\Psi_3^{(f,g)}$.

given by,

$$\mathbf{M} = \prod_{k=1}^{n_s} \left[\mathbf{H}_k \prod_{l=1}^{n_{\text{step}}} \mathbf{V}_{kl} \boldsymbol{\Theta} \mathbf{U}_{kl}^{*} \right], \tag{17}$$

being $\mathbf{V}_{kl}$ and $\mathbf{U}_{kl}$ random unitary matrices, with k and l denoting the span and the section, respectively, and the index $*$ denoting the Hermitian conjugate operator. The random unitary matrices are calculated using the orthogonal-triangular decomposition (QR factorization) [26]. In a single section, the modal dispersion can be written as

$$\boldsymbol{\Theta} = \text{diag}\left\{ e^{i\omega\tau_1}, ..., e^{i\omega\tau_{2n}} \right\}, \tag{18}$$

where τ_j is the group delay for the jth tributary signal. At the end of the kth span of fiber, an in-line amplifier enables to compensate the fiber losses. Moreover, in-line amplifiers can be tuned to compensate the losses of each spatial channel, which means that the MDL induced by the fibers can be neglected when compared with the ones induced by the optical amplifiers. In that way, the power imbalance at the end of the kth span of fiber plus the respective in-line amplifier can be written as [27],

$$\mathbf{H}_k = \text{diag}\left\{ e^{\frac{\rho_1^k(\omega)}{2}}, ..., e^{\frac{\rho_{2n}^k(\omega)}{2}} \right\}, \tag{19}$$

where $\vec{\rho^k} = (\rho_1^k, \rho_2^k, ...\rho_{2n}^k)$ follows a gaussian distribution with an average value of $\sum_{i=1}^{n} \rho_i^k = 0$ (measured in dB) and variance of σ^2. When assuming a large number of spans, the value of $\text{MDL}_{\text{P-P}}$ for the entire link can be approximately written as $\text{MDL}_{\text{P-P}} \approx \sqrt{n_s}\sigma$ [27].

Optics EXPRESS

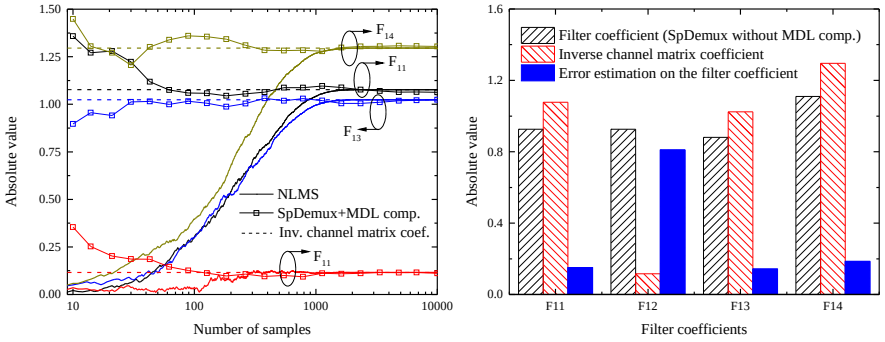

(a) (b)

Fig. 5. (a) Evolution of the absolute value of the filter coefficients for the NLMS and the HoPS-based SpDemux supported by the HoPS-based MDL equalizer. Dashed lines indicate the values of the inverse channel matrix. (b) Error estimation on the filter coefficients calculated by the HoPs-based SpDemux without MDL equalization. Sparse bars represents the filter coefficients calculated by the SpDemux algorithm without MDL equalization and the respective value of the inverse channel matrix. Parameter F denotes a given filter coefficient.

4.2. *Single MDL element and crosstalk*

Henceforward, independently of the statistics of the differential mode group delay, it is assumed that modal dispersion and chromatic dispersion can be compensated before the SpDemux stage assisted by the HoPs-based MDL equalization. In this subsection, we are going to assume that MDL is induced by a single element, i.e., the signal suffers of crosstalk after and before crossing the gain/loss dependent element. Thereby, in the multi-section propagation model, we considered a single MDL element described by Eq. (19) placed between two unitary transformation matrices. The estimated $MDL_{P\text{-}P}$ as a function of the fiber link MDL is shown in Fig. 3(a). We note that the proposed monitoring technique yields similar MDL values when considering different modulation formats (QPSK, 16QAM, and 64QAM), with a clear underestimation for the larger values of MDL. Indeed, the results show that for values higher than $\approx$ 6 dB, the error on the MDL estimation is higher than 0.5 dB, which can jeopardize the MDL monitoring and compensation. Figure 3(b) shows the estimated values for each component of the eigenvalues of the channel transfer matrix, considering a PM-QPSK modulated signal. In the range 0 to $\approx$ 6 dB of MDL, a good agreement is observed between the estimated and the real MDL values. Although not represented here, similar results were obtained for the other two modulation formats considered. Besides the $MDL_{P\text{-}P}$, the root means square (rms) value of the MDL vector has also been recently proposed as an alternative metric for the characterization of the MDL statistics of the SDM-based transmission system [4]. It should be noted that the entire MDL vector is accurately estimated by the proposed technique, and therefore the calculations of the rms values of the MDL vector can be also successfully done. In Fig. 3(a) and 3(b), the inaccuracies in the calculation of the MDL vector, evident in both figures, are related with the antisymmetric deformations induced by MDL, see Fig. 1. Henceforth, the value of 6 dB of $MDL_{P\text{-}P}$ is assumed as the maximum value of MDL considered in the following performance analyses.

As previously mentioned, the sample distribution in the HoPs is changed by crosstalk and MDL. Such distributions can be employed to deeply analyze the effect of the MDL compensation technique in the post-processed signal. With this aim in view, the Stokes parameters for the received signal, and the post-processed signal with and without considering the MDL compensation stage are compared with the B2B signal, see Fig. 4. The sample distributions

Optics EXPRESS

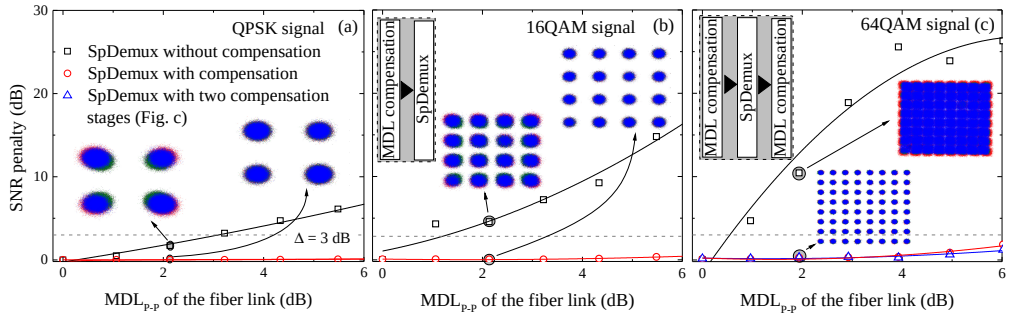

Fig. 6. SNR penalty as a function of the $MDL_{P\text{-}P}$ for a (a) PM-QPSK, (b) PM-16QAM and (c) PM-64QAM signals after space-demultiplexing with and without MDL compensation. Insets show both constellations with and without MDL compensation. It is assumed that MDL is induced by a single element.

analyzed in Fig. 4 are obtained from a PM-QPSK signal after propagated through a link with 3 dB of MDL. The histograms with the Stokes parameters for a given HoPs are grouped by columns. While, the histograms with the Stokes parameters, $\Psi_1^{(f,g)}$, $\Psi_2^{(f,g)}$ and $\Psi_3^{(f,g)}$, are shown in the upper, middle and lower rows, respectively. In dashed (black) line, it is drawn the histograms for the B2B signal, which are characterized by a symmetry around the origin of the HoPs. The histograms for the received signal are drawn in short dashed (blue) line. In this case, the aforementioned symmetry property is broken due to the crosstalk and MDL induced by the propagation along the link. In solid (green) line, it is shown the histograms for the post-processed signal without MDL compensation. The B2B and the post-processed signal have similar distributions, despite the average value for both distributions be different. However, when considered the MDL compensation stage in the DSP, the distributions of the signal samples post-processed match perfectly with the ones from the B2B signal. Hence the MDL-induced signal distortions were fully compensated, see the dotted (red) line in Fig. 4.

4.2.1. Convergence speed

In this subsection, we analyze the performance of the proposed technique in terms of convergence speed by comparing the evolution of the absolute value of the filter coefficients with the ones obtained by a normalized least mean square (NLMS) algorithm. In this analysis, we assume a SDM system with spatial diversity of 2, and a $MDL_{P\text{-}P}$ of 2 dB, where each spatial channel transmits a PM-QPSK signal. The HoPs-based DSP is composed by a HoPs-based MDL compensation stage followed by a SpDemux stage. In the SpDemux stage, it is assumed 150 samples in the calculations of the demultiplexing matrix. It should be noted that the implemented HoPs-based DSP does not have memory and therefore, in the NLMS algorithm, we used a single tap. The step size of the NLMS is chosen as 0.01 in order to achieve a good compromise between convergence speed and stability. Results show that both algorithms converge to the respective coefficient of the inverse channel see Fig. 5(a), with the HoPs requiring just 200 samples to reach a steady state, whereas the NLMS requires 5 times more samples (1000) to reach the same performance. Therefore, we can conclude that the convergence speed of the HoPs-based algorithms tends to be higher than a standard NLMS. Notice that the convergence speed of the NLMS can be increased by assuming a large value for the step size, however that will impose higher levels of noise in the calculations of the filter coefficients. In Fig. 5(b), it is shown the error estimation on the filter coefficients calculated by the HoPs-based SpDemux without MDL equalization for the channels considered in Fig. 5(a). The value of the filter coefficients calculated by the SpDemux algorithm without MDL equalization and the respective value of the inverse

Optics EXPRESS

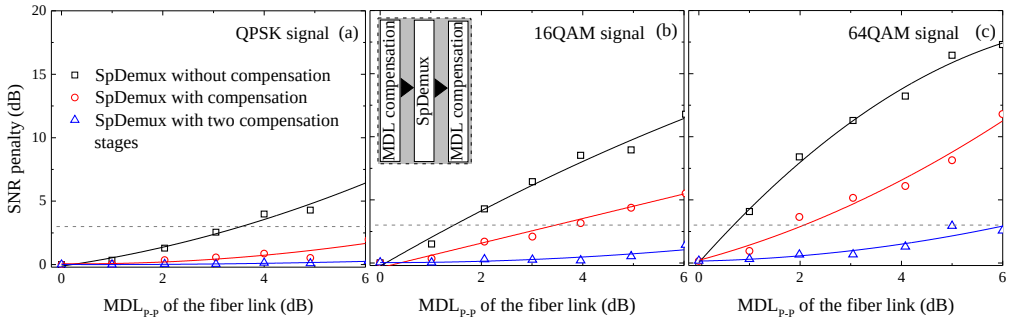

Fig. 7. SNR penalty as a function of the MDL$_{P-P}$ for a (a) PM-QPSK, (b) PM-16QAM and (c) PM-64QAM signals after space-demultiplexing without MDL compensation, with a MDL compensation stage and with two MDL compensation stages. It is assumed that MDL is distributed along the transmission channel.

channels matrix are represented by the sparse bars. In this case, the error on the calculation of the inverse channel matrix can be considerable. However, when the HoPs-based MDL compensation technique assists the SpDemux algorithm, the filter coefficients can be successfully calculated using only ~ 200 samples.

4.2.2. Performance assessment

In order to quantify the performance of the proposed technique, we used a figure of merit that compares the SNR of the signal launched in the fiber link with the SNR of the post-processed signal,

$$\Delta = \mathrm{SNR}_{in} - \mathrm{SNR}_{out}\,, \tag{20}$$

with Δ denoting the SNR penalty, and SNR_{in} and SNR_{out} being the SNR for the B2B and for the post-processed signal, respectively. For simplicity and without loss of generality, the following performance analysis is carried out as a function of the MDL$_{P-P}$. In Fig. 6, it is shown the SNR penalty after the SpDemux compensation stage as a function of the MDL$_{P-P}$, considering the cases with and without MDL compensation stages. Results show that MDL can substantially reduce the performance of the SpDemux stage inducing a severe SNR degradation in the post-processed signal, i.e., a MDL-sensitive algorithm. However, when the SpDemux is aided by a MDL compensation stage, the signal distortions arising from MDL are fully compensated. It should be emphasized that the remaining SNR penalty tends to increase with the value of MDL, in according with Fig. 3 due to the inherent limitations of the proposed technique, and with the density of the QAM constellation. Thus, the modulation format can apparently constrain the performance of the MDL compensation technique in the way that QAM constellations with higher density tends to require larger numbers of samples to accurately estimate the center of the constellation. Such limitations can be overcomed by using another MDL compensation stage placed after the SpDemux plus the MDL compensation stage. In Fig. 6(c), we employed an additional MDL compensation stage to enhance the calculation of the inverse channel matrix; therefore slightly improving the SNR penalty. The two MDL compensation stages are considered after and before of the SpDemux.

4.3. Channel with distributed MDL and crosstalk

In this subsection, we assume a link with 10 spans of fiber, each span comprising 10 sections. In the DSP, we assume three possible configurations: SpDemux without MDL compensation, SpDemux with a single MDL compensation stage, and SpDemux with two MDL compensation

Optics EXPRESS

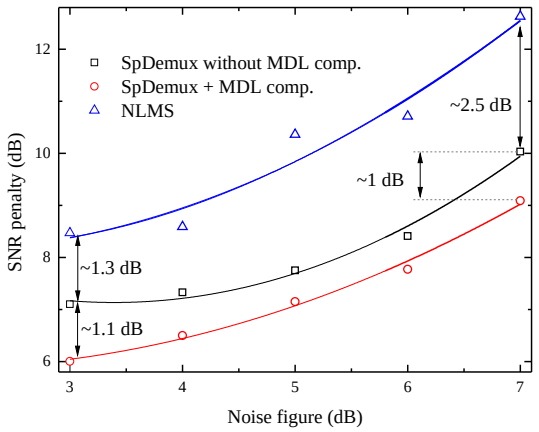

Fig. 8. SNR penalty as a function of the ASE. It is assumed a SDM transmission system with 10 spans of fiber and $MDL_{P\text{-}P}$ of 3 dB.

stages. The SNR penalty as a function of the $MDL_{P\text{-}P}$ is assessed for the three aforementioned configurations assuming the three modulation formats mentioned above, see Fig. 7. In the case of the PM-QPSK signal, the second MDL compensation stage slight enhance the SNR of the post-processed signal. On the other hand, when considered the PM-16QAM and the PM-64QAM signals, the remaining SNR penalty after a single MDL compensation stage still tends to be very high, see 7 (b) and (c). Nevertheless, the remaining penalty takes negligible values for the DSP configurations with two MDL compensation stage. In this case, the calculation of the inverse channels matrix is substantially improved by the two MDL compensation stages, which results in an almost negligible SNR penalty, see Fig. 7. We can conclude that when the transmission system has several elements with MDL, which corresponds to a more realistic scenario, the space-demultiplexing aided by the MDL compensation technique tends to require more than a single MDL compensation stage to successfully calculate the inverse channel matrix.

4.3.1. Channel with amplified spontaneous emission

In this subsection, the performance of the HoPs-based MDL compensation technique is analyzed for transmission channels with ASE; here modeled as additive Gaussian noise injected at the in-line amplifiers. It is assumed a transmission channel with spatial diversity of 2 and with $MDL_{P\text{-}P}$ of 3 dB, where each spatial channel transmits a PM-QPSK signal. The SDM link is composed of 10 spans of fiber (i.e., 10 in-line amplifiers) with noise figures ranging from 3 up to 7 dB. In Fig. 8, it is shown the SNR penalty of the post-processed signal for the HoPs-based SpDemux algorithm with and without MDL compensation technique and for a standard NLMS with one tap; these results are averaged over 10 trials. The step size of the NLMS is decreased for 0.005 and the length of the training sequence is increased to 2×10^5. We note that the filter coefficients calculated by the NLMS algorithm have considerable oscillations, which may be induced by ASE. On the other hand, the coefficients of HoPs-based SpDemux tend to be more stable and the performance of this algorithm tends to be better, which can be further improved by using the HoPs-based MDL compensation stage. The MDL compensation stage provides a SNR gain of $\approx$1 dB for all the cases considered. In that way, the HoPs-based DSP can apparently achieve a better performance than the NLMS algorithm. However, a detailed comparison of the proposed algorithm with other MDL insensitive algorithms is out of the scope of this paper.

Optics EXPRESS

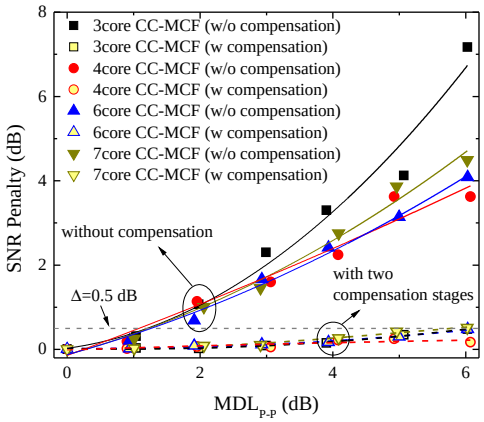

Fig. 9. SNR penalty as a function of the MDL_{P-P} for a SDM transmission system based on 3-, 4-, 6- and 7-core CC-MCF, in which each spatial channel supports a PM-QPSK signal. In the calculations of the inverse channels matrix, it is assumed two MDL compensation stages placed after and before the SpDemux.

4.3.2. Scalability

We also analyze the performance of the MDL compensation technique for several transmission systems with distinct degrees of spatial diversity, considering PM-QPSK signals. In Fig. 9, it is shown the SNR penalty as a function of the MDL for the aforementioned transmission system with a spatial diversity of 3, 4, 6 and 7, i.e., assuming a 3-, 4-, 6- and 7-core CC-MCF. When considered the two MDL compensation stages, the SNR penalty can be almost fully compensated independently of the number of spatial channels considered in the transmission system. Results show that the MDL compensation technique is independent of the number of channels supported by the SDM transmission system.

4.4. Brief considerations about practical implementation

It is well known from SSMF-based transmission systems that the Stokes-space DSP is quite sensitive to dispersion effects. Usually, these algorithms do not have "temporal memory" and therefore they are more suitable for the compensation of impairments without delayed time response, which is the case of crosstalk between polarization-multiplexed signals. In the presence of nonnegligible time-delay effects, suitable DSP subsystems able to equalize the dispersive effects are placed before Stokes-space based DSP [28–30]. In principle, a similar aproach can be also adopted in real SDM-based transmission systems with non-negligible values of modal dispersion, thus overcoming the possible performance limitations imposed by the dispersive effects. However, the impact of dispersive effects in the performance of the proposed technique is out of the scope of this paper.

The computational complexity of the proposed technique depends mainly on the calculation of the central point of the constellation. For a given HoPs, the number of real multiplications, N_{m}, and additions, N_{s}, required for such calculation can be expressed as

$$N_{\mathrm{m}} = 9n_s + 1\,, \tag{21a}$$

$$N_{\mathrm{s}} = 12n_s\,, \tag{21b}$$

with n_s denoting the number of samples used to compute the central point of the constellation. Notice that, these calculations must be performed over all the HoPs. On the other hand, the

Optics EXPRESS

number of HoPs depends on the degree of spatial diversity of the transmission systems, i.e., on the number of modes/cores. Hence, the complexity of the proposed algorithm scales quadraticaly with the number of spatial channels.

Usually, SDM systems tend to work at tens of GBaud while the characteristic time scales for MDL changes tend to be much bigger, on the order of tens of microseconds [31]. That means that in a practical implementation scenario, a significant number of samples can be considered in the calculations of the MDL, with these samples being updated in time scales shorter than tens of microsecond. In that way, the proposed technique can be suitable to track the MDL variations in real transmission systems. As previously mentioned, the accuracy of the proposed technique depends on the number of samples considered in the calculations of the central point, which, in turn, depends on the modulation format considered and on the SNR of the received signal.

5. Conclusion

We have proposed a new DSP technique for MDL monitoring and compensation in SDM-based transmission systems. This technique grounds on the representation of the signal samples on HoPs, shows practical scalability with the number of spatial channels, is modulation format agnostic and free of training sequences. The MDL vector is estimated by calculating the central point of the constellation over all the HoPs. Results showed that MDL-induced signal distortions can be successfully compensated by re-center all the constellations at the center of the respective HoPs. Indeed, the proposed technique allows to deal with MDL values as higher as 6 dB. Furthermore, the technique was successfully tested in scenarios with gain/losses power imbalance induced either by a single element or by several elements distributed along the link. In terms of SNR enhancements, when the HoPs-based SpDemux (a MDL-sensitive algorithm) is supported by the proposed MDL compensation technique, it provides a SNR gain of 2, 4 and 8 dB for PM-QPSK, PM-16QAM and PM-64QAM signals, respectively, assuming a SDM-based transmission system with 2 dB of MDL.

Funding

Fundação para a Ciência e a Tecnologia (FCT) (MCTechs POCI-01-0145-FEDER-029282, DSPMetroNet POCI-01-0145-FEDER-029405, and SFRH/BD/102631/2014).

Acknowledgments

The authors thank the reviewers for their suggestions and constructive comments, providing the opportunity to improve the paper. This work was supported in part by Fundação para a Ciência e a Tecnologia (FCT) through national funds MCTechs POCI-01-0145-FEDER-029282, and DSPMetroNet POCI-01-0145-FEDER-029405. The work of G. M. Fernandes was supported by the doctoral research under the grant SFRH/BD/102631/2014 by FCT.

References

1. R. Ryf and N. K. Fontaine, "Space-division multiplexing and MIMO processing," in *Enabling Technologies for High Spectral-Efficiency Coherent Optical Communication Networks*, X. Zhou and C. Xie, eds. (John Wiley & Sons, Ltd, 2016), 547–608.
2. A. Andrusier, M. Shtaif, C. Antonelli, and A. Mecozzi, "Assessing the effects of mode-dependent loss in space-division multiplexed systems," J. Light. Technol. **32**(7), 1317–1322 (2014).
3. G. Li, N. Bai, N. Zhao, and C. Xia, "Space-division multiplexing: the next frontier in optical communication," Adv. Opt. Photonics **6**(4), 413–487 (2014).
4. K. Choutagunta, S. Ö. Arik, K. Ho, and J. M. Kahn, "Characterizing mode-dependent loss and gain in multimode components," J. Light. Technol. **36**(18), 3815–3823 (2018).
5. S. J. Savory, "Digital coherent optical receivers: algorithms and subsystems," IEEE J. Sel. Top. Quantum Electron **16**(5), 1164–1179 (2010).

Optics EXPRESS

6. H. Li, G. Huang, Z. Tao, H. Chen, S. Oda, Y. Akiyama, T. Yamauchi, and T. Hoshida, "An accurate and robust PDL monitor by digital signal processing in coherent receiver," in *Optical Fiber Communications Conference and Exposition (OFC),* (2018), pp. M2F–6.
7. N. J. Muga and A. N. Pinto, "Digital PDL compensation in 3D Stokes space," J. Light. Technol. **31**(13), 2122–2130 (2013).
8. B. Szafraniec, B. Nebendahl, and T. Marshall, "Polarization demultiplexing in Stokes space," Opt. Express **18**(17), 17928–17939 (2010).
9. Z. Yu, X. Yi, Q. Yang, M. Luo, J. Zhang, L. Chen, and K. Qiu, "Polarization demultiplexing in Stokes space for coherent optical PDM-OFDM," Opt. Express **21**(3), 3885–3890 (2013).
10. S. Ziaie, N. J. Muga, F. P. Guiomar, G. M. Fernandes, R. M. Ferreira, A. Shahpari, A. L. Teixeira, and A. N. Pinto, "Experimental assessment of the adaptive Stokes space-based polarization demultiplexing for optical metro and access networks," J. Light. Technol. **33**(23), 4968–4974 (2015).
11. G. Bosco, M. Visintin, P. Poggiolini, A. Nespola, M. Huchard, and F. Forghieri, "Experimental demonstration of a novel update algorithm in Stokes space for adaptive equalization in coherent receivers," in *European Conference on Optical Communication (ECOC),* (2014), pp. Tu.3.3.6.
12. S. Ziaie, R. Ferreira, N. J. Muga, F. P. Guiomar, A. Shahpari, A. Teixeira, and A. N. Pinto, "Coherent UDWDM transceivers based on adaptive Stokes space polarization de-multiplexing in real-time," in *European Conference on Optical Communication (ECOC),* (2017), pp. Th.1.B.4.
13. N. J. Muga and A. N. Pinto, "Adaptive 3-D Stokes space-based polarization demultiplexing algorithm," J. Light. Technol. **32**(19), 3290–3298 (2014).
14. J. N. Damask, *Polarization optics in telecommunications* (Springer Science & Business Media, 2004).
15. D. Naidoo, F. S. Roux, A. Dudley, I. Litvin, B. Piccirillo, L. Marrucci, and A. Forbes, "Controlled generation of higher-order Poincaré sphere beams from a laser," Nat. Photonics **10**(5), 327–332 (2016).
16. G. Milione, H. I. Sztul, D. A. Nolan, and R. R. Alfano, "Higher-order Poincaré sphere, Stokes parameters, and the angular momentum of light," Phys. Rev. Lett. **107**(5), 053601 (2011).
17. A. Holleczek, A. Aiello, C. Gabriel, C. Marquardt, and G. Leuchs, "Classical and quantum properties of cylindrically polarized states of light," Opt. Express **19**(10), 9714–9736 (2011).
18. D. Aerts and M. Sassoli de Bianchi, "The extended Bloch representation of quantum mechanics: Explaining superposition, interference, and entanglement," J. Math. Phys. **57**(12), 122110 (2016).
19. G. M. Fernandes, N. J. Muga, and A. N. Pinto, "Space-demultiplexing based on higher-order Poincaré spheres," Opt. Express **25**(4), 3899–3915 (2017).
20. G. M. Fernandes, N. J. Muga, and A. N. Pinto, "Reduced-complexity algorithm for space-demultiplexing based on higher-order Poincaré spheres," Opt. Express **26**(10), 13506 (2018).
21. C. Antonelli, A. Mecozzi, M. Shtaif, and P. J. Winzer, "Stokes-space analysis of modal dispersion in fibers with multiple mode transmission," Opt. Express, **20**(11) 11718-11733 (2012).
22. F. J. Vaquero Caballero, A. Zanaty, F. Pittala, G. Goeger, Y. Ye, I. Tafur Monroy, and W. Rosenkranz, "Efficient SDM-MIMO Stokes-space equalization," in *European Conference on Optical Communication (ECOC),* (2016), pp. 1–3.
23. D. Soma, Y. Wakayama, K. Igarashi and T. Tsuritani, "Weakly-coupled FMF transmission for reduction of MIMO complexity," in *IEEE Photonics Society Summer Topical Meeting Series*, (2016), pp. 140–141.
24. T. Hayashi, R. Ryf, N. K. Fontaine, C. Xia, S. Randel, R.-J. Essiambre, P. J. Winzer, and T. Sasaki, "Coupled-core multi-core fibers: High-spatial-density optical transmission fibers with low differential modal properties," in *European Conference on Optical Communication (ECOC),* (2015), pp. 0318.
25. D. L. Butler, "Space-division multiplexing (SDM) technology for short-reach fiber optic systems," in *Optical Fiber Communications Conference and Exposition (OFC)*, 2016, p. Tu3I.1.
26. F. Mezzadri, "How to generate random matrices from the classical compact groups," Notices AMS, **54**(5), 592–604 (2007).
27. K.-P. Ho and J. M. Kahn, "Linear propagation effects in mode-division multiplexing systems," J. Light. Technol. **32**(4), 614–628 (2014).
28. F. Buchal, H. Bulow, K. Schuh, and W. Idler, "4D-CMA: Enabling separation of channel compensation and polarization demultiplex," in *Optical Fiber Communications Conference and Exposition (OFC),* (2015), p. Th2A.15.
29. B. Szafraniec, T. S. Marshall, and B. Nebendahl, "Performance monitoring and measurement techniques for coherent optical systems," J. Light. Technol. **31**(4), 648–663 (2013).
30. S. Ziaie, F. P. Guiomar, N. J. Muga, A. Nespola, G. Bosco, A. Carena and A. N. Pinto, "Adaptive Stokes-based polarization demultiplexing for long-haul multi-subcarrier systems," IEEE Photonic Tech. L., **31**(10), 759–762 (2019).
31. S. Ö. Arik, D. Askarov and J. M. Kahn, "Adaptive frequency-domain equalization in mode-division multiplexing systems," J. Light. Technol. **32**(10), 1841–1852 (2014).